Published in final edited form as:
Cancer Res. 2012 February 15; 72(4): 990–1000. doi:10.1158/0008-5472.CAN-11-2688.

Histone deacetylase inhibition increases levels of choline kinase alpha and phosphocholine facilitating non-invasive imaging in human cancers

Mounia Beloueche-Babari[1], **Vaitha Arunan**[1], **Helen Troy**[1], **Robert H te Poele**[3], **Anne-Christine Wong Te Fong**[1], **L Elizabeth Jackson**[1], **Geoffrey S Payne**[1], **John R Griffiths**[2], **Ian R Judson**[3], **Paul Workman**[3], **Martin O Leach**[1,*], and **Yuen-Li Chung**[1]

[1]Cancer Research UK and EPSRC Cancer Imaging Centre, Division of Radiotherapy and Imaging, The Institute of Cancer Research and The Royal Marsden NHS Foundation Trust, Sutton, Surrey SM2 5PT, UK

[2]Cancer Research UK Cambridge Research Institute, Li Ka Shing Centre, Cambridge CB2 ORE, UK

[3]Cancer Research UK Cancer Therapeutics Unit, Division of Cancer Therapeutics, The Institute of Cancer Research, Sutton, Surrey SM2 5NG, UK

Abstract

Histone deacetylase (HDAC) inhibitors are currently approved for cutaneous T-cell lymphoma and are in mid-late stage trials for other cancers. The HDAC inhibitors LAQ824 and SAHA increase phosphocholine (PC) levels in human colon cancer cells and tumor xenografts as observed by magnetic resonance spectroscopy (MRS). In this study, we show that belinostat, an HDAC inhibitor with an alternative chemical scaffold, also caused a rise in cellular PC content that was detectable by ^{1}H and ^{31}P MRS in prostate and colon carcinoma cells. In addition, ^{1}H MRS showed an increase in branched chain amino acid and alanine concentrations. ^{13}C-choline labeling indicated that the rise in PC resulted from increased *de novo* synthesis and correlated with an induction of choline kinase α (ChoKα) expression. Furthermore, metabolic labeling experiments with ^{13}C-glucose showed that differential glucose routing favored alanine formation at the expense of lactate production. Additional analysis revealed increases in the choline/water and phosphomonoester (including PC)/total phosphate ratios *in vivo*. Together, our findings provide mechanistic insights into the impact of HDAC inhibition on cancer cell metabolism and highlight PC as a candidate non-invasive imaging biomarker for monitoring the action of HDAC inhibitors.

Keywords

HDAC; targeted cancer therapy; mechanism of action; non-invasive metabolic biomarkers; choline

[*]**Correspondence:** (martin.leach@icr.ac.uk) Cancer Research UK and EPSRC Cancer Imaging Centre, Division of Radiotherapy and Imaging, The Institute of Cancer Research and The Royal Marsden NHS Foundation Trust, Sutton, Surrey SM2 5PT, UK. Phone: +44 (0) 208 661 3338 Fax: +44 (0) 208 0846 .

Disclosure of potential conflicts of interest: M.B-B., V.A., R.T., A-C.W., L.E.J., I.R.J, P.W., M.O.L. and Y-L.C. are employees of The Institute of Cancer Research, which has a commercial interest in HDAC inhibitors and which operates a “rewards to inventors” scheme. Paul Workman was a founder of Chroma Therapeutics and is Chairman of its Scientific Advisory Board.

Europe PMC Funders Author Manuscripts

INTRODUCTION

Histone acetylation is a key regulator of eukaryotic gene expression which controls DNA accessibility to transcription factors and mRNA transcription. The histone acetylation/deacetylation balance is maintained by the opposing activities of histone acetyl transferases and histone deacetylases (HDACs) resulting in cell-specific gene expression patterns (1). Deregulation of histone acetylation results in abnormal gene expression profiles involved in controlling cell proliferation, differentiation and apoptosis, and is associated with malignancy (2-5).

HDACs also act on other non-histone proteins that are subject to regulation by acetylation including some transcription factors (e.g. E2F) and the heat shock protein 90 (HSP90) molecular chaperone, which maintains the conformational stability of several oncogenic proteins (e.g. ErbB2) (6).

HDAC inhibition is a promising anti-tumor approach for simultaneously targeting multiple oncogenic players and pathways. Several HDAC inhibitors have been described that induce potent anti-tumor effects in cells and tumor xenografts (6-8). The HDAC inhibitors SAHA (vorinostat) and depsipeptide FK228 (romidepsin) have gained FDA approval for cutaneous T-cell lymphoma treatment and many more are currently under clinical evaluation (6;8-11). One example is belinostat which has shown promising activity in pre-clinical cancer models and in patients (8;12).

The development and evaluation of novel HDAC inhibitors requires the identification and validation of pharmacodynamic (PD) biomarkers of drug activity. These are important because they inform on the inhibition of the intended biochemical target, help assess response dynamics, aid treatment schedule and dose planning, and subsequently allow therapeutic efficacy assessment (13-15). In contemporary drug development, non-invasive endpoints of target modulation are highly desirable as they do not involve surgical intervention and allow longitudinal studies in the same patient to be performed (15-17).

Non-invasive imaging of cancer metabolism is a valuable approach for PD biomarker discovery that exploits the altered metabolic features of tumors relative to normal tissues, including increased lipid synthesis and aerobic glycolysis (18;19). These metabolic changes are increasingly being investigated as diagnostic as well as treatment response biomarkers, with techniques such as magnetic resonance spectroscopy (MRS) being of particular value for translating findings from pre-clinical models to humans (16;17;20-22).

MRS allows the detection of many metabolites (e.g. those related to glucose, protein and lipid metabolism), and in pre-clinical studies has shown that response to molecularly-targeted therapeutics is often associated with altered metabolism (17;20). For example, inhibitors of HSP90 (23;24), phospholipase Cγ1 (25), mitogen activated protein kinase MEK (26) or phosphoinositide 3-kinase (27;28) have all been shown to alter choline phospholipid metabolism in human cancer cells. In the case of the HDAC inhibitor LAQ824, *in vitro* and *in vivo* MRS showed increased phosphocholine (PC) levels both in human colon cancer cells and tumors post-treatment (29). A similar effect was also observed in human colon and prostate cancer cells treated with the HDAC inhibitor SAHA (29) or its fluoro-analogue (30), respectively. Furthermore, LAQ824 treatment caused a substantial reduction in tumor bioenergy-related metabolites (e.g. NTP, glucose) that was observed *in vivo* but not *in vitro* (29). This effect was attributed to the anti-angiogenic action of LAQ824, while the rise in PC was likely to relate to the effect of HDAC inhibition on tumor cell metabolism (29) although the molecular and biochemical mechanisms behind this change remain unclear.

Here we assess i) whether similar metabolic effects would be observed with the alternative chemotype (chemical scaffold) HDAC inhibitor and probe compound belinostat, and ii) the molecular and biochemical processes underlying the observed metabolic alterations.

We show that HDAC inhibition with belinostat in human cancer cells leads to increased alanine and branched-chain amino acid (BCAA) content that was associated with altered glucose utilization. Belinostat also increased PC levels, thus confirming our previous finding with the alternative chemotype agent LAQ824. Importantly, we show for the first time that this effect is associated with induction of choline kinase α (ChoKα) gene and protein expression. The increase in PC is also observed in belinostat-treated tumors *in vivo,* thus supporting the role of PC as a potential non-invasive metabolic imaging biomarker of HDAC inhibition.

MATERIALS AND METHODS

Cell culture

Human HT29 colon and PC3 prostate carcinoma cells (ATCC) were grown in DMEM or RPMI, respectively, containing 10% FBS, 100U/ml penicillin and 100μg/ml streptomycin in a 37°C humidified 5% CO_2 atmosphere. Cells were preserved and propagated according to ATCC's protocols, screened monthly for mycoplasma and passaged for no longer than three months. All cell culture materials were from Life Technologies (Paisley, UK).

Western blotting

Analysis of the molecular effects of HDAC inhibition was performed using Western blotting as previously described (29). The primary antibodies rabbit anti-acetyl histone-3 (Millipore; Watford, UK), rabbit anti-choline kinase alpha (ChoKα, Sigma-Aldrich; Dorset, UK), mouse anti-GAPDH (Chemicon; Hampshire, UK) and rabbit α-tubulin (Cell Signaling Technology; Danvers, MA, USA) were used. The secondary anti-rabbit and anti-mouse antibodies were from GE Healthcare Life Sciences (Buckinghamshire, UK).

Growth inhibition and cell cycle analysis

Cell counts were performed on a Beckman Coulter Vi-Cell® Cell Viability Analyzer. The impact of belinostat on cell proliferation and cell cycle distributions was assessed using the sulforhodamine B (SRB) assay and flow cytometry, respectively, as previously described (27).

Cell treatment for *in vitro* MRS

PC3 and HT29 cells were treated for 24h with belinostat (0.9μM and 2μM, respectively), to obtain a 30-50% reduction in cell counts and induction of histone-3 acetylation as a characteristic molecular biomarker of HDAC inhibition (9).

HT29 cells were further treated with 2μM belinostat for 4h and 16h to assess response time dynamics. Control cells were treated with 0.01% DMSO.

For ^{13}C-tracer experiments, HT29 cells were treated as above for 16h followed by a further 3h incubation in fresh medium containing DMSO or 2μM belinostat and 28μM [1,2-^{13}C]-choline (Cambridge Isotope Laboratories; Andover, MA, USA-final concentration 56μM) or 5mM [1-^{13}C]-glucose (Sigma Aldrich-final concentration 25mM). At the end of treatment, cells were extracted using a dual phase method (26), and samples lyophilized for MRS analysis.

Quantitative real time (qRT) PCR

Total RNA was extracted using the RNAeasy kit (Qiagen; Crawley, West Sussex, UK) and 500 nanogram was reverse transcribed using the High Capacity cDNA Reverse Transcription Kit (Applied Biosystems; Carlsbad, California, USA). Samples were diluted 1:5 and 1μl used in the Taqman assay, using Taqman universal master mix, and the Hs03682798_m1 assay for the ChoKα gene *CHKA* (*CHKA* specific primers and FAM labeled probe) multiplexed with the 4326314E assay for large ribosomal protein 0 gene *LRP0* (*LRP0* specific primers and VIC labeled probe, Applied Biosystems). mRNA levels of *CHKA* and *LRP0* were determined for each sample in the same well on the ABI 7900HT. *CHKA* mRNA levels were expressed relative to those of *LRP0*.

HT29 human colon tumor xenograft model

MF-1 male nude mice were injected subcutaneously in the flank with 5×10^6 HT29 human colon carcinoma cells. Tumor volume was calculated by measuring the length, width, and depth using calipers and the formula $L\times W\times D\times(\pi/6)$. Once an appropriate tumor volume (~350mm^3) was established (3-4 weeks later), mice were randomized into two groups; one group was treated with belinostat in vehicle (10% DMSO in water) at 60mg/kg p.o. once a day for 3 days (days 1, 2 &3, n=13), and one group was treated with vehicle alone (n=12). A cohort of animals (6 vehicle- and 6 belinostat-treated) was used in the MRS study, and tumors were excised on day 3 for Western blotting or *in vitro* MRS. Another animal cohort (6 vehicle- and 7 belinostat-treated) was used to study tumor growth delay where animals were treated as above and tumor volumes monitored for a further 6 days after the last dose. Animals were treated in accordance with local and national ethical requirements and with the UK National Cancer Research Institute (NCRI) Guidelines for the Welfare and Use of Animals in Cancer Research (31).

In vivo MRS of HT29 tumors

Mice were anesthetized as previously described (29) and scanned in a 7T Bruker Magnetic Resonance System spectrometer with tumors positioned in the center of a 15-mm two-turn ^{1}H/^{31}P surface coil. *In vivo* localized PRESS ^{1}H MRS (TE=136 ms and TR=4 s) and image-selected spectroscopy (ISIS) ^{31}P MRS (TR=2s) of the tumors were carried out before treatment (day 0) and the last day of treatment (day 3). ^{1}H and ^{31}P MR spectra were quantified using jMRUI as previously described (24). After the final scan, tumors were excised and stored at -80°C for subsequent *in vitro* MRS or Western blotting.

The surface coils used to obtain the ^{31}P MRS signal from subcutaneous tumors *in vivo* have a non-uniform spatial sensitivity making it difficult to normalize to an external standard. Therefore, the signal intensities observed by *in vivo* ^{31}P MRS are expressed as metabolite ratios.

In vitro MRS of tumor extracts

Freeze-clamped HT29 tumors (~200mg) were extracted in 6% ice-cold PCA as previously described (29). Neutralized extracts were freeze-dried and reconstituted in 1ml of D_2O and 0.5ml was then analyzed. Sodium 3-trimethylsilyl-2,2,3,3-tetradeuteropropionate (TSP; 50μl, 5mM) was added as an internal chemical shift and quantification reference. The pH of the samples was re-neutralized with PCA or KOH followed by acquisition of water-suppressed ^{1}H MRS spectra. For ^{31}P MRS, EDTA (50μl, 60mM) was added to chelate metals ions, and methylenediphosphonic acid (internal reference; 50μl, 5mM) was added.

In vitro MRS of cell extracts and media samples

Lyophilized samples of the aqueous fraction of cell extracts were processed as above. The lipid phase of cell extracts was reconstituted in $CDCl_3$ containing 0.56mM trimethyl silane (internal standard). Media samples from the [1-^{13}C]-glucose experiments were prepared by adding 50μl D2O and 50μl TSP (5mM, internal reference) to 0.45ml of medium. ^{1}H and ^{31}P spectra were acquired as previously described (23). ^{13}C MR spectra were acquired using power gated composite pulse ^{1}H decoupling, a 30° flip angle, a 2s repetition delay, a spectral width of 220ppm and 32K data points. Spectral processing and metabolite quantitation were performed as previously described (23).

Statistical analysis

Statistical significance was assessed using Student's *t*-tests with $p \leq 0.05$ considered to be significant. Pearson correlation analysis was performed using GraphPad Prism version 5.01. Data represent the mean±SE.

RESULTS

Belinostat treatment alters cellular metabolism in human HT29 and PC3 carcinoma cells

Belinostat inhibited proliferation in HT29 colon and PC3 prostate cancer cells as shown by the SRB assay (Table S1). The respective exposure of HT29 and PC3 cells to 2μM ($5\times GI_{50}$) and 0.9μM ($3\times GI_{50}$) belinostat for 24h led to a substantial reduction in cell counts to 57±3% and 77±2% of controls, respectively ($p \leq 0.001$). Western blotting demonstrated the induction of histone-3 acetylation post-treatment with belinostat consistent with HDAC inhibition in both cell lines (Figure 1A). Significant alterations in cell cycle profiles were observed after belinostat treatment characterized by a build up in the G1 and G2/M cell populations concomitant with a reduction in the S phase fraction in HT29 cells (Figure S1).

To evaluate the metabolic effects of HDAC inhibition we analyzed the ^{1}H and ^{31}P MR spectra from the aqueous fractions of HT29 and PC3 cell extracts post-treatment with belinostat.

Relative to controls, ^{1}H MRS revealed time-dependent increases in PC levels in HT29 cell extracts which were also present in PC3 cells following a 24 h exposure to belinostat (Figure 1B & C). Decreased glycerophosphocholine (GPC) levels were also recorded in HT29 cells at 16h and 24h, and PC3 cells at 24h; nevertheless, the total choline (tCho) signal comprising PC+GPC remained higher, relative to controls, following belinostat treatment in both cell lines (Figure 1C).

In addition, we also observed time-dependent increases in levels of the branched-chain amino acids (BCAA, comprising valine, leucine and isoleucine), alanine and threonine in belinostat-treated HT29 cells compared to controls (Figure 1B & C). Similar effects on BCAA and alanine were also observed in PC3 cells at 24h following belinostat treatment (Figure 1C).

^{31}P MRS analysis confirmed the ^{1}H MRS observed changes showing that, relative to controls, PC levels were not significantly altered at 4h (19±3 vs 19±2 fmol/cell, n=3) but increased significantly at 16h (17±2 vs 25±2 fmol/cell; n=5, p=0.02) and 24 h (18±1 vs 27±2 fmol/cell; n=6, p=0.0003). GPC levels decreased significantly at 16h (7±1 vs 4±1 fmol/cell, p=0.02) and 24h (8±1 vs 6±1 fmol/cell, p=0.03) post-treatment. Data from the 24h time point are further summarized in Table 1, which also shows a similar increase in PC levels in PC3 cells treated with belinostat.

^{1}H MRS analysis of the lipid fraction of HT29 cell extracts indicated that phosphatidylcholine (PtdCho) levels, determined by integrating the N-trimethyl resonance at 3.2ppm, increased from 204±18 arbitrary units/cell to 290±28 arbitrary units/cell following belinostat treatment (n=4, p=0.04).

HDAC inhibition with belinostat alters glucose utilization

To investigate the basis for the rise in amino acid (AA) levels, HT29 cells were cultured in the presence of [1-^{13}C]-glucose for 3h to monitor tracer uptake and incorporation into glycolytic intermediates.

^{13}C MRS of cell extracts indicated that, following belinostat treatment, no significant effects were observed on intracellular ^{13}C-glucose levels; however, extracellular [3-^{13}C]-lactate (measured by ^{13}C MRS of cell culture media) decreased markedly to 25±11% relative to controls (n=4, p=0.007). Interestingly, the reduction in ^{13}C-lactate production was paralleled with a significant rise, by almost 3-fold, in the amount of the ^{13}C label incorporated into [3-^{13}C]-alanine as shown in Figure 2A and B. A slight reduction in intracellular [3-^{13}C]-lactate and increase in [4-^{13}C]-glutamate were also noted but neither of these effects reached statistical significance (p≥0.2). The [4-^{13}C]-glutamate/[3-^{13}C]-lactate ratio, however, increased by almost 3-fold (p=0.03).

Altogether, these data suggest that belinostat treatment induced a shift in glucose routing, leading to a reduction in glucose flux to lactate in favor of a rise in alanine formation.

HDAC inhibition with belinostat increases *de novo* PC synthesis and induces ChoKα expression

To investigate the basis for the PC rise, HT29 cells were cultured in the presence of [1,2-^{13}C]-choline to monitor label incorporation into PC post-vehicle or belinostat treatment.

^{13}C MRS of the aqueous fraction of cell extracts following a 3h incubation in ^{13}C-choline indicated that the levels of ^{13}C-labelled PC, synthesized from the incorporation of ^{13}C-choline, increased to 155±12% in belinostat-treated cells relative to controls (Figure 3A and B, p=0.01). This degree of increase is comparable to the fold rise in PC recorded by ^{31}P and ^{1}H MRS, suggesting that the effect on the steady state levels of this metabolite is due to increased *de novo* formation.

To characterize the molecular drivers of this effect, we assessed the expression of ChoKα, the enzyme that catalyses the formation of PC from its precursor choline. qRT-PCR analysis indicated that following belinostat treatment the levels of ChoKα mRNA were induced by 2.3-fold at 4h, 3.5-fold at 16h and 3.2-fold at 24h relative to controls in HT29 cells (Figure 3C) and this effect correlated strongly with the increase in PC levels observed by MRS (r=0.99, p=0.02). ChoKα mRNA was also induced to 148±8% relative to controls (n=9, p=0.002) in PC3 cells following a 24h treatment with belinostat. Western blotting of the HT29 cell samples from the ^{13}C-choline labeling experiment showed induction of ChoKα protein expression up to 260±45% (n=3, p=0.018) of controls following exposure to belinostat (Figure 3D).

HDAC inhibition with belinostat increases levels of choline-containing metabolites of HT29 xenografts *in vivo*

To assess if any of the metabolic alterations observed in cells would be translatable to *in vivo* tumor models, we evaluated the metabolite profiles of HT29 tumor xenografts following treatment with belinostat.

Europe PMC Funders Author Manuscripts

Following 3 days of treatment, tumor volumes increased by 20±3% in the vehicle- and 3±2% in the belinostat-treated group ($p<0.0001$) (Figure 4A). After therapy cessation, tumor growth inhibition in the belinostat-treated group became statistically insignificant relative to controls by day7 (Figure 4A). Western blots of the excised tumors following 3 days of treatment showed increased histone-3 acetylation in the belinostat-treated group (Figure 4B), thus confirming the expected inhibitory effect of belinostat on HDAC in HT29 xenografts.

In vivo ^{1}H MR spectra from a HT29 tumor pre- and post-belinostat treatment are shown in Figure 4C (left panel) where resonances from tCho and lipids can be observed. A significant increase (169±25% of post-/pre-treatment values, $p=0.02$) in tCho/water ratio was observed in the belinostat-treated group. The tCho/water ratio did not change significantly in the vehicle-treated group (89±7% of post-/pre-treatment values, $p=0.26$).

In vivo ^{31}P MR spectra from a HT29 tumor pre- and post-belinostat treatment are shown in Figure 4C (right panel), where resonances from phosphomonoesters (PME), phosphodiesters (PDE), inorganic phosphate (Pi), α-, β-, γ- NTP and phosphocreatine (PCr) can be observed. Significant increases in PME/TotP (total phosphorus signal) ($p=0.01$) and Pi/TotP ratios ($p=0.03$) were observed post-belinostat treatment (Table 2A). No significant change in metabolite ratios was observed in the vehicle-treated group (Table 2B).

In vitro high resolution ^{1}H and ^{31}P MRS analyses of HT29 tumor extracts showed elevated PC ($p=0.04$), GPC ($p=0.04$) and free choline ($p=0.01$) levels, and reduced glucose ($p=0.01$) and formate levels in belinostat-treated HT29 tumor extracts relative to vehicle-treated tumors (Table 3A) as detected by ^{1}H MRS. ^{31}P MRS analysis showed increased PC ($p=0.03$) and GPC ($p=0.05$) levels in belinostat-treated tumors (Table 3B) relative to controls, consistent with the *in vivo* ^{1}H and ^{31}P MRS changes.

DISCUSSION

HDAC inhibitors are targeted anti-cancer agents currently approved for cutaneous T-cell lymphoma and in mid-late stage trials for other cancers (1;10;11). The development of such agents requires the discovery and validation of biomarkers, and particularly those that are non-invasive, to monitor target modulation and aid treatment planning and evaluation.

Imaging of tumor metabolism is a promising approach for biomarker discovery as it exploits the distinct metabolic characteristics of the tumor to inform on its behavior following therapy (17;20-22). Moreover, studying tumor metabolism informs on the metabolic pathways modulated by targeted agents thereby providing a means for investigating potential mechanisms of action.

Using MRS, we have previously shown that HDAC inhibition with LAQ824 leads to increased PC levels in HT29 human colon carcinoma cells *in vitro* and tumors *in vivo* (29). The aims of this study were to i) confirm this observation using belinostat in HT29 cells *in vitro* and *in vivo* in addition to PC3 human prostate cancer cells *in vitro*, and ii) investigate the mechanism(s) underlying this effect.

The clinical development of belinostat is now primarily directed towards the use of this drug in combination with chemotherapy. In this study belinostat served as an alternative chemotype probe to the agents currently in the clinic. Probe compounds have considerable value for interrogating the molecular function of target proteins and the downstream biological processes they mediate, and for biomarker discovery and validation (32).

HT29 and PC3 cells were treated *in vitro* with belinostat at a concentration and duration that led to target modulation (shown by histone-3 hyperacetylation) and inhibition of cell

proliferation (shown by SRB assays and cell counts). ^{31}P MRS metabolic analysis under these conditions indicated that the most significant effect observed in both HT29 and PC3 cells after 24h of treatment was a rise in PC content, which was time-dependent in HT29 cells. When detectable (in HT29 cells), GPC levels decreased post-belinostat treatment. The changes in PC and GPC were confirmed by ^{1}H MRS which also indicated that the tCho signal was also significantly higher following belinostat treatment in both cell lines. The rise in PC is in line with our previous findings with LAQ824 and SAHA in HT29 cells (29) indicating that it is not inhibitor chemotype-specific or cell line/tissue type-dependent.

Furthermore, belinostat treatment resulted in increased BCAAs, alanine and threonine levels in both HT29 and PC3 cells as shown by ^{1}H MRS. These changes were also time-dependent in HT29 cells.

Next we set out to investigate the metabolic processes underlying the increases in AA and PC levels following HDAC inhibition. An increase in AAs could reflect i) elevated uptake, ii) increased *de novo* formation from glycolytic intermediates or other AAs, iii) increased proteolysis, iv) decreased utilization (e.g. in protein synthesis), or a combination of the above.

Measurement of HT29 cell lysates by the BIO-RAD method revealed a 10% rise in protein content of belinostat-treated cells relative to controls (data not shown). Therefore it is unlikely that the rise in AAs observed here could reflect increased proteolysis or decreased protein synthesis as this would be expected to reduce the overall cellular protein mass.

To assess whether AA rise was due to increased synthesis from glycolytic intermediates, we analyzed the ^{13}C MRS profiles of belinostat-treated cells incubated in [1-^{13}C]-glucose for 3h. This short incubation time ensured that the ^{13}C-labelled metabolites detected were formed directly from the ^{13}C-glucose precursor rather than other pre-labeled metabolic intermediates.

This experiment revealed increases in ^{13}C-glucose-derived ^{13}C-alanine (up to ~3-fold) which coincided with decreased ^{13}C-lactate production by up to 75% of controls. Moreover, there was a trend towards an increase in cellular ^{13}C-glutamate and ^{13}C-glucose although neither of these effects was statistically significant.

Taken together, these observations suggest that belinostat treatment led to differential metabolic routing that favors the conversion of pyruvate to alanine at the expense of lactate synthesis.

A previous report showed inhibition of glucose transport concomitant with reduced hexokinase activity following HDAC inhibition (33). Here we did not observe a reduction in ^{13}C-glucose accumulating in the cells, and the combined level of downstream ^{13}C-intermediates (lactate+alanine+glutamate) formed from ^{13}C-glucose appeared to be comparable between control and treated cells (Figure 2A and B). These observations suggest that glucose uptake was probably unaltered under our experimental conditions although more work is required to test this hypothesis.

Furthermore, and although neither of the changes in individual content of intracellular ^{13}C-lactate or ^{13}C-glutamate following belinostat treatment were statistically significant, the [4-^{13}C]-glutamate/[3-^{13}C]-lactate ratio increased by ~3-fold. This effect could suggest an altered balance between glycolysis and Krebs cycle metabolism as previously reported (34).

Next we investigated the basis for the PC rise following belinostat treatment. PC is formed via two main routes: i) *de novo* synthesis through ChoK-catalyzed phosphorylation of its

precursor choline and ii) release from membrane PtdCho via PtdCho-specific phospholipase C or release of choline from PtdCho via phospholipase D followed by ChoK-mediated phosphorylation (35).

To distinguish these two processes, we assessed levels of ^{13}C-PC in cells incubated in [1,2-^{13}C]-choline for 3h. This short duration ensured that the ^{13}C-PC observed was formed *de novo* from exogenous ^{13}C-choline, thus excluding contributions from membrane PtdCho-derived PC (since the ^{13}C-choline would take much longer than 3h to be incorporated into PtdCho and then be released again (36)).

^{13}C MRS indicated that levels of ^{13}C-PC formed were ~1.5-fold higher in belinostat-treated cells relative to controls. The amplitude of this increase is similar to that observed by ^{1}H and ^{31}P MRS indicating that the elevation in steady state PC is driven primarily by increased *de novo* synthesis.

To further delineate the molecular processes driving this effect we assessed the expression of ChoKα. qRT-PCR analysis revealed an induction in ChoKα gene expression in HT29 cells which correlated strongly with the rise in PC levels measured by MRS and which was also confirmed by ChoKα protein expression in these cells. A similar increase in ChoKα expression was also observed in PC3 cells, albeit to a lesser extent. These findings point to the induction of ChoKα expression as a key driver of the rise in PC observed by MRS following belinostat treatment in both HT29 and PC3 cells.

PtdCho levels increased by ~1.4-fold in belinostat-treated HT29 cells relative to controls, as shown by ^{1}H MRS, indicating that the *de novo* formed PC was used to supply PtdCho synthesis. This finding concurs with the previously reported role of HDAC inhibition in inducing the expression of CTP-PC cytidylyltransferase, the rate limiting enzyme in PtdCho biosynthesis of (37). Interestingly, levels of GPC, which is a PtdCho breakdown product, fell post-belinostat treatment in cells (but not tumors), suggesting that HDAC inhibition probably also inhibited PtdCho degradation, which together with activation of the synthetic pathway led to net augmentation in this membrane phospholipid. However, this effect did not translate to increases in cell volume (90-110% of control), suggesting that PtdCho was not used to synthesize new outer cell membrane and that it was probably deployed to other cellular compartments. More work is required to establish the significance of the rise in PtdCho following belinostat treatment, assess the effect of therapy on other lipid species and define the involvement of PtdCho metabolizing enzymes (e.g. phospholipase A2, C and D) in the MRS changes observed here.

The induction in ChoKα observed following HDAC inhibition and the ensuing increase in PC are unusual and, paradoxically, more commonly associated with malignancy (38). Indeed ChoKα expression is linked to oncogene activation (39) and correlates with poor patient prognosis (40). Further studies are required to elucidate the significance of the choline metabolism effects observed here in relation to HDAC inhibitor-induced anti-tumor activity.

Finally, and to assess whether any of the changes observed in cancer cells could serve as potential non-invasive biomarkers of HDAC inhibition, we investigated the effect of belinostat in tumor xenografts derived from the same HT29 cells used *in vitro*. *In vivo* ^{1}H MRS revealed increased tCho/water ratio following belinostat treatment. Although therapy-induced changes in water content can contribute to a rise in tCho/water, increased PME/TotP was also observed by *in vivo* ^{31}P MRS following treatment with belinostat. Furthermore, e*x vivo* MRS revealed increased PC and GPC levels in belinostat-treated tumors relative to controls. This indicates that the *in vivo* MRS-detectable changes are primarily due to increased PC and GPC content in the drug-treated group.

The rise in PC concurs with our *in vitro* cell observations and with our previous findings with LAQ824 and SAHA (29), indicating that this effect is likely to be associated with the mechanism of action of HDAC inhibitors. We also found an increase in tumor GPC following belinostat treatment but a decrease in GPC was observed in belinostat-treated cells and previously in LAQ824-treated tumor extracts (29).

Interestingly, although HDAC inhibition led to significant increases in cellular AA levels and previously in HT29 tumors *in vivo* post-LAQ824 treatment (29), no significant effects on AA content were recorded in the belinostat-treated tumors. The basis for this difference is unclear and may relate to drug-induced physiologic effects that may vary under the different treatment conditions.

In line with our previous findings with LAQ824 (29), glucose concentration fell in the belinostat-treated tumors compared to controls albeit to a lesser extent compared to LAQ824 (35% vs 61%). This effect did not correlate with major changes in tumor bioenergy metabolites as seen with LAQ824 (29). The differences in bioenergetic effects between the two HDAC inhibitors may be due to the additional anti-vascular effects of LAQ824 (41).

In summary, we show that the most consistent and reproducible metabolic signature observed following HADC inhibition in cells and *in vivo* tumors is increased PC levels. Importantly, we show for the first time that this effect is driven by increased *de novo* formation involving up-regulation of ChoKα mRNA and protein expression.

Further studies are required to delineate the precise molecular links between HDAC and ChoKα expression, and to unravel the significance of the choline metabolic effects in relation to drug-induced anti-cancer activity. Our findings also support the role of PC as a potentially useful non-invasive metabolic imaging biomarker for monitoring the action of HDAC-targeted therapeutics.

Supplementary Material

Refer to Web version on PubMed Central for supplementary material.

Acknowledgments

We thank Dr SP Robinson for help with setting up the *in vivo* MRS facility. Belinostat was generously provided by TopoTarget and the National Cancer Institute, NIH. Paul Workman is a Cancer Research UK Life Fellow.

GRANT SUPPORT We acknowledge the support received for the Cancer Research UK and EPSRC Cancer Imaging Centre in association with the MRC and Department of Health (England) grant#C1060/A10334. We also acknowledge support from Cancer Research UK project grant#C1060/6916 and programme grant#C309/A8274, and NHS funding to the NIHR Biomedical Research Centre.

Financial support: We acknowledge the support received for the Cancer Research UK and EPSRC Cancer Imaging Centre in association with the MRC and Department of Health (England) grant # C1060/A10334. We also acknowledge support from Cancer Research UK project grant # C1060/6916 and program grant # C309/A8274, and NHS funding to the NIHR Biomedical Research Centre.

REFERENCES

1. Marks P, Rifkind RA, Richon VM, Breslow R, Miller T, Kelly WK. Histone deacetylases and cancer: causes and therapies. Nat Rev Cancer. 2001; 1(3):194–202. [PubMed: 11902574]
2. Cress WD, Seto E. Histone deacetylases, transcriptional control, and cancer. J Cell Physiol. 2000; 184(1):1–16. [PubMed: 10825229]

Europe PMC Funders Author Manuscripts

3. Wade PA. Transcriptional control at regulatory checkpoints by histone deacetylases: molecular connections between cancer and chromatin. Hum Mol Genet. 2001; 10(7):693–8. [PubMed: 11257101]
4. Weichert W, Roske A, Gekeler V, Beckers T, Ebert MP, Pross M, et al. Association of patterns of class I histone deacetylase expression with patient prognosis in gastric cancer: a retrospective analysis. Lancet Oncol. 2008; 9(2):139–48. [PubMed: 18207460]
5. Weichert W. HDAC expression and clinical prognosis in human malignancies. Cancer Lett. 2009; 280(2):168–76. [PubMed: 19103471]
6. Lane AA, Chabner BA. Histone deacetylase inhibitors in cancer therapy. J Clin Oncol. 2009; 27(32):5459–68. [PubMed: 19826124]
7. Paris M, Porcelloni M, Binaschi M, Fattori D. Histone deacetylase inhibitors: from bench to clinic. J Med Chem. Mar 27; 2008 51(6):1505–29. [PubMed: 18247554]
8. Tan J, Cang S, Ma Y, Petrillo RL, Liu D. Novel histone deacetylase inhibitors in clinical trials as anti-cancer agents. J Hematol Oncol. 2010; 3:5. [PubMed: 20132536]
9. de Bono JS, Kristeleit R, Tolcher A, Fong P, Pacey S, Karavasilis V, et al. Phase I pharmacokinetic and pharmacodynamic study of LAQ824, a hydroxamate histone deacetylase inhibitor with a heat shock protein-90 inhibitory profile, in patients with advanced solid tumors. Clin Cancer Res. 2008; 14(20):6663–73. [PubMed: 18927309]
10. Ramalingam SS, Maitland ML, Frankel P, Argiris AE, Koczywas M, Gitlitz B, et al. Carboplatin and Paclitaxel in combination with either vorinostat or placebo for first-line therapy of advanced non-small-cell lung cancer. J Clin Oncol. 2010; 28(1):56–62. [PubMed: 19933908]
11. Ma X, Ezzeldin HH, Diasio RB. Histone deacetylase inhibitors: current status and overview of recent clinical trials. Drugs. 2009; 69(14):1911–34. [PubMed: 19747008]
12. Ramalingam SS, Belani CP, Ruel C, Frankel P, Gitlitz B, Koczywas M, et al. Phase II study of belinostat (PXD101), a histone deacetylase inhibitor, for second line therapy of advanced malignant pleural mesothelioma. J Thorac Oncol. 2009; 4(1):97–101. [PubMed: 19096314]
13. Banerji U, de Bono J, Judson I, Kaye S, Workman P. Biomarkers in early clinical trials: the committed and the skeptics. Clin Cancer Res. 2008; 14(8):2512–4. [PubMed: 18413847]
14. Carden CP, Banerji U, Kaye SB, Workman P, de Bono JS. From darkness to light with biomarkers in early clinical trials of cancer drugs. Clin Pharmacol Ther. 2009; 85(2):131–3. [PubMed: 19151637]
15. Yap TA, Sandhu SK, Workman P, de Bono JS. Envisioning the future of early anticancer drug development. Nat Rev Cancer. 2010; 10(7):514–23. [PubMed: 20535131]
16. Workman P, Aboagye EO, Chung YL, Griffiths JR, Hart R, Leach MO, et al. Minimally invasive pharmacokinetic and pharmacodynamic technologies in hypothesis-testing clinical trials of innovative therapies. J Natl Cancer Inst. 2006; 98(9):580–98. [PubMed: 16670384]
17. Beloueche-Babari M, Chung YL, Al-Saffar NM, Falck-Miniotis M, Leach MO. Metabolic assessment of the action of targeted cancer therapeutics using magnetic resonance spectroscopy. Br J Cancer. 2010; 102(1):1–7. [PubMed: 19935796]
18. Deberardinis RJ, Lum JJ, Hatzivassiliou G, Thompson CB. The biology of cancer: metabolic reprogramming fuels cell growth and proliferation. Cell Metab. 2008; 7(1):11–20. [PubMed: 18177721]
19. Tennant DA, Duran RV, Boulahbel H, Gottlieb E. Metabolic transformation in cancer. Carcinogenesis. 2009; 30(8):1269–80. [PubMed: 19321800]
20. Beloueche-Babari M, Workman P, Leach MO. Exploiting tumor metabolism for non-invasive imaging of the therapeutic activity of molecularly targeted anticancer agents. Cell Cycle. 2011; 10(17):2883–93. [PubMed: 21857160]
21. Aboagye EO. Phosphatidylcholine metabolic transformation and progression signature as a pharmacodynamic biomarker. Oncotarget. 2010; 1(3):163–6. [PubMed: 21301046]
22. Witney TH, Brindle KM. Imaging tumour cell metabolism using hyperpolarized 13C magnetic resonance spectroscopy. Biochem Soc Trans. 2010; 38(5):1220–4. [PubMed: 20863288]
23. Beloueche-Babari M, Arunan VA, Jackson LE, Perusinghe N, Sharp SY, Workman P, et al. Modulation of melanoma cell phospholipid metabolism in response to heat shock protein 90 inhibition. Oncotarget. 2010; 1(3):185–97. [PubMed: 21037799]

Europe PMC Funders Author Manuscripts

24. Chung YL, Troy H, Banerji U, Jackson LE, Walton MI, Stubbs M, et al. Magnetic resonance spectroscopic pharmacodynamic markers of the heat shock protein 90 inhibitor 17-allylamino,17-demethoxygeldanamycin (17AAG) in human colon cancer models. J Natl Cancer Inst. 2003; 95(21):1624–33. [PubMed: 14600095]
25. Beloueche-Babari M, Peak JC, Jackson LE, Tiet MY, Leach MO, Eccles SA. Changes in choline metabolism as potential biomarkers of phospholipase C{gamma}1 inhibition in human prostate cancer cells. Mol Cancer Ther. 2009; 8(5):1305–11. [PubMed: 19417158]
26. Beloueche-Babari M, Jackson LE, Al-Saffar NM, Workman P, Leach MO, Ronen SM. Magnetic resonance spectroscopy monitoring of mitogen-activated protein kinase signaling inhibition. Cancer Res. 2005; 65(8):3356–63. [PubMed: 15833869]
27. Beloueche-Babari M, Jackson LE, Al-Saffar NM, Eccles SA, Raynaud FI, Workman P, et al. Identification of magnetic resonance detectable metabolic changes associated with inhibition of phosphoinositide 3-kinase signaling in human breast cancer cells. Mol Cancer Ther. 2006; 5(1): 187–96. [PubMed: 16432178]
28. Al-Saffar NM, Jackson LE, Raynaud FI, Clarke PA, Ramirez de MA, Lacal JC, et al. The phosphoinositide 3-kinase inhibitor PI-103 downregulates choline kinase alpha leading to phosphocholine and total choline decrease detected by magnetic resonance spectroscopy. Cancer Res. 2010; 70(13):5507–17. [PubMed: 20551061]
29. Chung YL, Troy H, Kristeleit R, Aherne W, Jackson LE, Atadja P, et al. Noninvasive magnetic resonance spectroscopic pharmacodynamic markers of a novel histone deacetylase inhibitor, LAQ824, in human colon carcinoma cells and xenografts. Neoplasia. 2008; 10(4):303–13. [PubMed: 18392140]
30. Sankaranarayanapillai M, Tong WP, Maxwell DS, Pal A, Pang J, Bornmann WG, et al. Detection of histone deacetylase inhibition by noninvasive magnetic resonance spectroscopy. Mol Cancer Ther. 2006; 5(5):1325–34. [PubMed: 16731766]
31. Workman P, Aboagye EO, Balkwill F, Balmain A, Bruder G, Chaplin DJ, et al. Guidelines for the welfare and use of animals in cancer research. Br J Cancer. 2010; 102(11):1555–77. [PubMed: 20502460]
32. Workman P, Collins I. Probing the probes: fitness factors for small molecule tools. Chem Biol. 2010; 17(6):561–77. [PubMed: 20609406]
33. Wardell SE, Ilkayeva OR, Wieman HL, Frigo DE, Rathmell JC, Newgard CB, et al. Glucose metabolism as a target of histone deacetylase inhibitors. Mol Endocrinol. 2009; 23(3):388–401. [PubMed: 19106193]
34. Poptani H, Bansal N, Jenkins WT, Blessington D, Mancuso A, Nelson DS, et al. Cyclophosphamide treatment modifies tumor oxygenation and glycolytic rates of RIF-1 tumors: 13C magnetic resonance spectroscopy, Eppendorf electrode, and redox scanning. Cancer Res. 2003; 63(24):8813–20. [PubMed: 14695197]
35. Podo F. Tumour phospholipid metabolism. NMR Biomed. 1999; 12(7):413–39. [PubMed: 10654290]
36. Katz-Brull R, Margalit R, Bendel P, Degani H. Choline metabolism in breast cancer; 2H-, 13C- and 31P-NMR studies of cells and tumors. MAGMA. 1998; 6(1):44–52. [PubMed: 9794289]
37. Banchio C, Lingrell S, Vance DE. Role of histone deacetylase in the expression of CTP:phosphocholine cytidylyltransferase alpha. J Biol Chem. 2006; 281(15):10010–5. [PubMed: 16484221]
38. Glunde K, Jie C, Bhujwalla ZM. Molecular causes of the aberrant choline phospholipid metabolism in breast cancer. Cancer Res. 2004; 64(12):4270–6. [PubMed: 15205341]
39. Ramirez De Molina A, Penalva V, Lucas L, Lacal JC. Regulation of choline kinase activity by Ras proteins involves Ral-GDS and P13K. Oncogene. 2002; 21(6):937–46. [PubMed: 11840339]
40. Ramirez de Molina A, Sarmentero-Estrada J, Belda-Iniesta C, Taron M, Ramirez De Molina V, Cejas P, et al. Expression of choline kinase alpha to predict outcome in patients with early-stage non-small-cell lung cancer: a retrospective study. Lancet Oncol. 2007; 8(10):889–97. [PubMed: 17851129]
41. Qian DZ, Wang X, Kachhap SK, Kato Y, Wei Y, Zhang L, et al. The histone deacetylase inhibitor NVP-LAQ824 inhibits angiogenesis and has a greater antitumor effect in combination with the

vascular endothelial growth factor receptor tyrosine kinase inhibitor PTK787/ZK222584. Cancer Res. 2004; 64(18):6626–34. [PubMed: 15374977]

Europe PMC Funders Author Manuscripts

Europe PMC Funders Author Manuscripts

Précis

Non-invasive biomarkers offer critical tools for clinical trials of targeted drugs, as illustrated in this study providing mechanistic support for the use of phosphocholine as a candidate non-invasive biomarker for imaging the pharmacodynamic response to HDAC inhibitors.

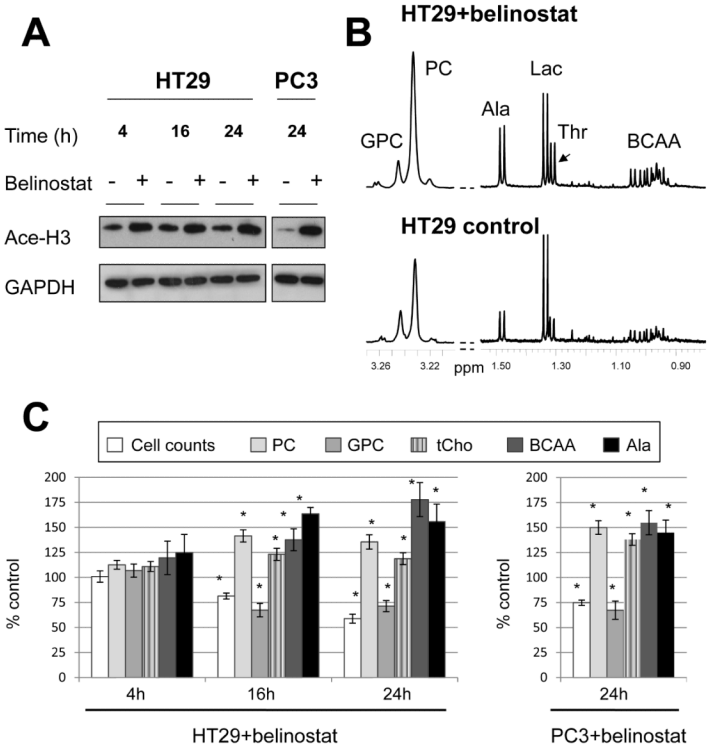

Figure 1.

The effect of HDAC inhibition with belinostat on histone-3 acetylation and ^{1}H MRS-detectable cellular metabolites. A) Western blots showing increased acetyl histone-3 (Ace-H3) following belinostat treatment in HT29 (2μM for 4h, 16h and 24h) and PC3 cells (0.9μM for 24h). B) Representative ^{1}H MR spectra showing levels of choline-containing metabolites and amino acids in control and belinostat-treated (2μM, 24h) HT29 cells. C) Changes relative to control in the ^{1}H MRS-detectable metabolites following belinostat treatment in HT29 (4h, 16h and 24h, 2μM) and PC3 cells (24h, 0.9μM). *:$p<0.05$. GPC:glycerophosphocholine, PC:phosphocholine, Ala:alanine, Lac:lactate, Thr:threonine, BCAA:branched-chain amino acids, tCho:total choline.

Europe PMC Funders Author Manuscripts

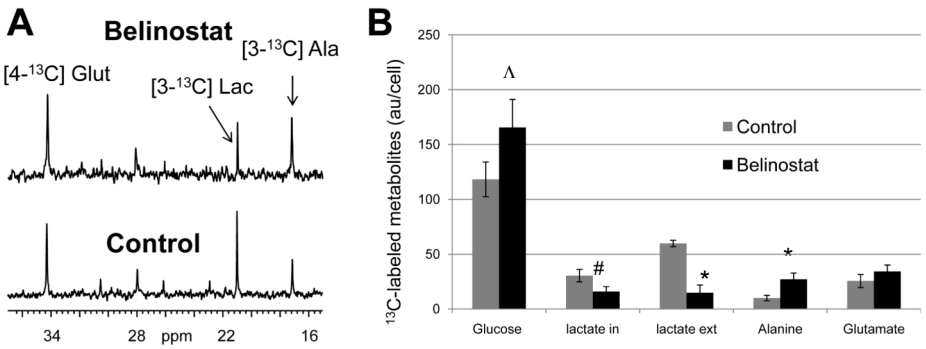

Figure 2.

The effect of belinostat treatment (16h+3h) on ^{13}C-glucose utilization in HT29 human colon cancer cells. A) ^{13}C spectra of HT29 cells incubated in [1-^{13}C]-glucose for 3h showing the effect of belinostat treatment (2μM) on [4-^{13}C]-glutamate (Glut), [3-^{13}C]-lactate (Lac) and [3-^{13}C]-alanine (Ala). B) Quantitation of ^{13}C-labelled glucose, lactate (intra- and extracellular), alanine and glutamate in control and belinostat-treated HT29 cells following a 3h incubation in [1-^{13}C]-glucose showing increased alanine formation and decreased lactate production.

Europe PMC Funders Author Manuscripts

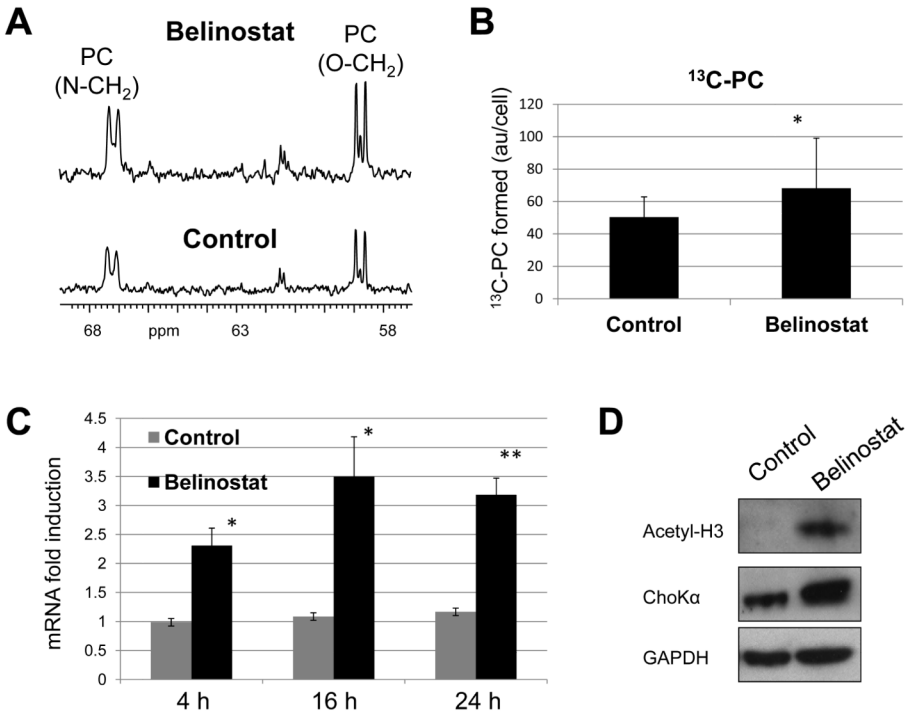

Figure 3.

The effect of belinostat treatment on ^{13}C-PC synthesis and ChoKα expression in HT29 human colon cancer cells. A) ^{13}C spectra showing the increase in ^{13}C-PC signals following belinostat treatment (2μM) of cells grown in [1,2]-^{13}C choline. B) Quantitation of *de novo* ^{13}C-PC levels in control and belinostat-treated HT29 cells. *p=0.04. C) The effect of treatment with 2μM belinostat for 4h, 16h and 24h on ChoKα mRNA levels determined by qRT-PCR. D) Western blots showing increased ChoKα protein expression concomitant with acetyl histone-3 (Ace-H3) induction following a 16h+3h treatment with 2μM belinostat.

Europe PMC Funders Author Manuscripts

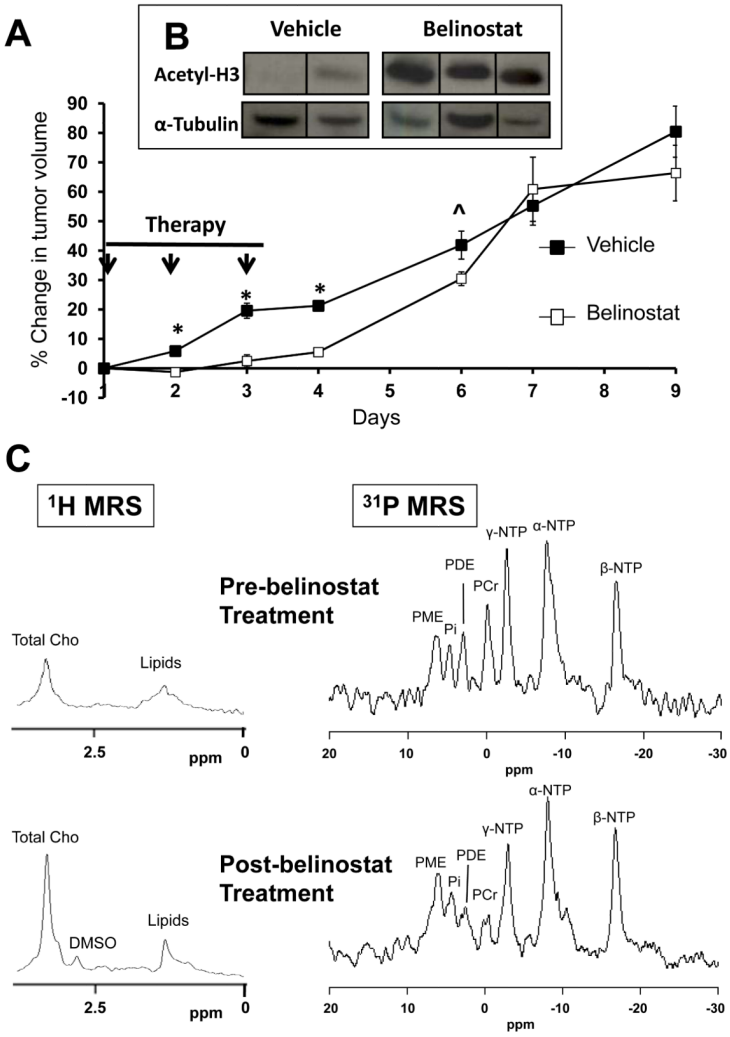

Figure 4.

The effects of belinostat treatment on growth, acetyl histone-3 levels and *in vivo* MRS profiles in HT29 tumor xenografts. A) Changes in HT29 tumor volumes (relative to day 1) following 3 days of treatment with vehicle (filled squares; n=12 at day 1, 2 and 3 and n=6 thereafter) or 60mg/kg belinostat (open squares; n=13 at day 1, 2, and 3 and n=7 thereafter). *p<0.001 and ^p=0.06 comparing belinostat-treated with controls. B) Western blots for acetyl histone-3 (Ace-H3) in HT29 xenografts following 3 days treatment with vehicle or belinostat. C) *In vivo* ^{1}H and ^{31}P MR spectra of HT29 tumors pre- and post-belinostat treatment. Total Cho:total choline, PME:phosphomonoesters, PDE:phosphodiesters, Pi:inorganic phosphate, PCr:phosphocreatine, a-, b-, g-NTP:nucleotide triphosphates.

Europe PMC Funders Author Manuscripts

Europe PMC Funders Author Manuscripts

Table 1

The effect of the HDAC inhibitor belinostat on the ^{31}P-containing aqueous metabolites in human HT29 colorectal and PC3 prostate carcinoma cells following a 24h exposure to 2μM and 0.9μM, respectively.

Metabolites (fmol/cell)	HT29 (n=6)			PC3 (n=4)		
	Control	Belinostat	p‡	Control	Belinostat	p‡
PC	18±1	27±1	0.0003	17±1	24±1	0.003
PE	ND	ND	-	7±1	8±1	0.08
GPC	8±1	6±1	0.03	ND	ND	-
GPE	2±1	3±1	0.37	ND	ND	-
NTP	8±1	8±1	0.86	10±1	11±2	0.69

PC:phosphocholine, PE:phosphoethanolamine, GPC:glycerophosphocholine, GPE:glycerophosphoethanolamine, NTP:nucleotide triphosphate.

‡Two-tailed unpaired t-test comparing changes between control and belinostat-treated cells.

ND: not detectable.

Europe PMC Funders Author Manuscripts

Table 2

In vivo ^{31}P MRS of HT29 tumors

A) Pre- and post-belinostat treatment (n=6)

Metabolite ratios	Pre-belinostat	Post-belinostat	*p* ‡
PME/TotP	0.13±0.01	0.15±0.01	0.01
β-NTP/TotP	0.22±0.02	0.21±0.02	NS
β-NTP/Pi	5.28±1.35	3.01±0.93	0.02
Pi/TotP	0.05±0.02	0.10±0.01	0.03

B)Pre- and post-vehicle treatment (n=6)

Metabolite ratios	Pre-Vehicle	Post-Vehicle	p ‡
PME/TotP	0.14±0.02	0.12±0.01	NS
β-NTP/TotP	0.21±0.02	0.23±0.01	NS
β-NTP/Pi	4.10±1.86	6.16±1.43	NS
Pi/TotP	0.09±0.02	0.05±0.01	NS

‡Two-tailed paired t-test comparing changes pre- and post-belinostat treatment within the same group of animals.

NS: p>0.1.

Table 3

In vitro MRS of HT29 tumors

A) ^{1}H MRS

Metabolites (μmol/g w.wt)	Control (n=6)	Belinostat (n=6)	p ‡
PC	2.57±0.25	3.33±0.21	0.04
GPC	2.29±0.17	3.02±0.26	0.04
Free choline	0.04±0.01	0.06±0.01	0.01
Glucose	0.79±0.07	0.51±0.07	0.01
Formate	0.24±0.05	0.13±0.02	0.05
Lactate	8.35±1.01	7.20±1.00	NS

B) ^{31}P MRS

Metabolites (μmol/g w.wt)	Control (N = 5)	Belinostat (N = 5)	p ‡
PE	1.48 ± 0.06	1.96 ± 0.27	0.09
PC	1.85 ± 0.12	2.59 ± 0.25	0.03
GPE	0.99 ± 0.10	1.17 ± 0.08	NS
GPC	1.78 ± 0.22	2.39 ± 0.06	0.05
Pi	3.86 ± 0.29	4.06 ± 0.23	NS

‡Two-tailed unpaired t-test comparing changes between vehicle- and belinostat-treated groups.

NS: p>0.1.